Microstructural Banding and Failure of a Stainless Steel

A.C. STAUFFER, D.A. KOSS, and J.B. McKIRGAN

The presence of microstructural bands in AL-6XN stainless steel plate has been examined. The bands, which consist of a high density of second-phase particles, are located near the midthickness of the plate, range in thickness up to 300 μm, and are continuous over lengths up to 50 mm. Chemical analyses of the microstructural bands indicate elevated levels of chromium and molybdenum, while orientation imaging microscopy identified primarily sigma-phase particles within the bands; a small volume fraction of chi phase was also found. Tensile specimens oriented in the short transverse direction of the plate show low ductility and exhibit a large variation in failure strains, depending on the continuity of the bands as well as the presence of large precipitate particles within the bands. When oriented in either the longitudinal or the long transverse direction of the plate, circumferentially notched tensile specimens exhibit comparatively high ductility, although at high stress triaxialities, the material was susceptible to specimen *splitting* parallel to the tensile axis due to cracking along microstructural bands.

I. INTRODUCTION

SOLUTE segregation during casting of alloys is a common occurrence. For steels processed by casting and hot rolling, the segregation of substitutional alloying elements during the dendritic solidification often results in microstructural banding (References 1 through 6, for example). In low-alloy steels, the presence of significant amounts of manganese, chromium, and molybdenum causes solidification to occur over a large range of both temperatures and compositions with the result that the interdendritic regions have a high solute content. During subsequent rolling, these regions become elongated and can take the form of chemical or composition bands aligned parallel to the rolling direction. Upon cooling, the differences in solute chemistry between the high solute bands and the neighboring material then results in *microstructural banding* within the plate.

Austenitic stainless steels are commonly known for their toughness and corrosion resistance. Of these steels, AL-6XN* is commonly referred to as a "super-austenitic" stainless steel with a high Ni content (24 wt pct Ni) and, importantly, it contains a significant amount of Mo (6 wt pct) in addition to the level of Cr (20-21 wt pct) typical of austenitic grades.[7] Given certain thermal histories, some stainless steels may be susceptible to the formation of potentially detrimental intermetallic phases, such as the sigma phase.[7–13] A key to the formation of sigma is the presence of high levels of Cr and Mo.[14,15] In contrast, elements such as carbon, nickel, and nitrogen retard its formation,[7,10,14,] and significantly, AL-6XN has a relatively high nitrogen content (0.2 wt pct).

The relatively high levels of Cr and Mo in the AL-6XN alloy suggest the possibility of rejection of these elements to the interdendritic regions during the solidification process. For the case of steels in the form of a relatively thick hot-rolled plate, chemistry differences near the plate centerline might exist, resulting in bands of high Mo as well as Cr content. The purpose of this study is to identify the presence of microstructural banding that occurred in AL-6XN plate (12.7 mm) and that was induced by high levels of Cr and Mo concentrated near the midthickness of the plate. The characteristics of the microstructural bands, the phases present, and the examples of the resulting effects on the tensile fracture behavior of AL-6XN will be presented.

*AL-6XN is a registered trademark of ATI Properties, Inc., Pittsburgh, PA.

A.C. STAUFFER, formerly Graduate Student with the Department of Materials Science and Engineering, Pennsylvania State University, is Materials Engineer, Naval Surface Warfare Center, Carderock Division, West Bethesda, MD 20817. D.A. KOSS, Professor, is with Department of Materials Science and Engineering, Pennsylvania State University, University Park PA 16802. Contact e-mail: koss@ems.psu.edu. J.B. McKIRGAN, Mechanical Engineer, is with the Naval Surface Warfare Center, Carderock Division.

Manuscript submitted June 5, 2003.

II. EXPERIMENTAL PROCEDURE

This study is based on the superaustenitic stainless steel AL-6XN in the form of 12.7-mm-thick base plate provided by the Naval Surface Warfare Center, Carderock Division (NSWCCD). The material was processed from 20-cm-thick continuously cast slab, and after hot deformation, it was solution annealed at a temperature $\geq$1107 °C, and rapidly cooled. The composition of the plate is listed in Table I.

The initial investigation began with an analysis of the fracture behavior of circumferentially notched tensile samples that contained notches of varying radii similar to the specimen geometries used initially by Hancock and Mackenzie and subsequently by others.[16–19] The specimens had a maximum diameter of 8.96 mm and a minimum diameter in the notched section of $2R = 4.54$ mm with notch severities that ranged from $R/\rho = 0.25$ to 2.0, where ρ is the notch root radius. Eight specimens were tested in each condition with tensile axes oriented either in the rolling direction of the plate or transverse to the rolling direction (and in the plane of the plate). In addition to the circumferentially notched specimens, seven smooth tensile specimens oriented in the short transverse direction of the plate were also tested. Limited by the 12.7-mm thickness of the plate, these specimens had a 4.4-mm gage diameter and a 6.6-mm gage length. In all cases, tests were performed at an initial strain rate of approximately 10^{-3}/s.

In order to examine the microstructural banding, metallographic specimens were prepared by grinding, polishing, and etching using one of two etching solutions. The general

Table I. Composition of AL-6XN Base Plate

Element	C	Mn	P	S	Si	Cr	Ni	Mo	N	Cu	Co	Fe
Wt pct	0.024	0.41	0.021	0.0004	0.36	20.56	23.84	6.21	0.213	0.2	0.2	47.86

microstructural features were examined after etching in a modified glyceregia reagent consisting of a mixture of nitric acid (10 mL), glacial acetic acid (10 mL), hydrochloric acid (15 mL), and glycerol (3 mL). In addition, a modified ASTM A 262 (oxalic acid) etch test was used by placing the specimen in a solution of oxalic acid with a potential of 6 V for approximately 4 seconds. This latter procedure has been used to detect sigma phase precipitation in AL-6XN.[7]

In addition to conventional light microscopy and scanning electron microscopy (SEM), electron probe microanalysis (EPMA) was used to determine (and compare) the chemistries of the matrix and microstructural bands. Three polished and etched samples were prepared for this chemical analysis by placing microhardness indents on either side of a banded region to mark the area for a trace to be completed. The EPMA tests were performed at Carpenter Technology Corporation (Reading, PA) using a Cameca SX-50 (Cameca Instruments, Inc., Trumbull, CT) instrument that conducted a 100-point line scan every 7 μm for a total distance of 700 μm. Data reporting the elemental weight percent of various elements were obtained as a function of distance across the specimen.

The technique used to identify the precipitates within the microstructural bands was orientation imaging microscopy (OIM) using an MIT DE1000 SIT system (TSL/EDAX, Draper, UT). This technique was used in accordance with SEM with a system capable of automatically indexing electron backscatter diffraction patterns, thereby allowing one to identify a particular phase based on pattern identification.[20,21] The chemistry and crystal structure of potential phases were input into the OIM software, which determined whether the diffraction patterns obtained (matched) the input data, and if so, the accuracy of the match as indicated by a confidence index value. The OIM was performed on a scale such that second-phase particles of a size roughly greater than 0.4 μm could be identified.

Specimen preparation for the OIM involved the standard metallographic techniques used for polishing, after which the samples were finally polished using colloidal silica for 20 minutes to obtain a lightly etched specimen surface. Microhardness indents were placed on either side of the banded region in order to locate the precipitate phase in the SEM.

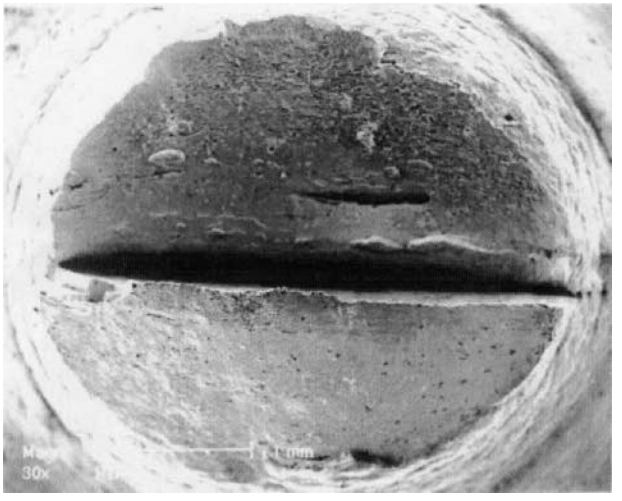

(*a*)

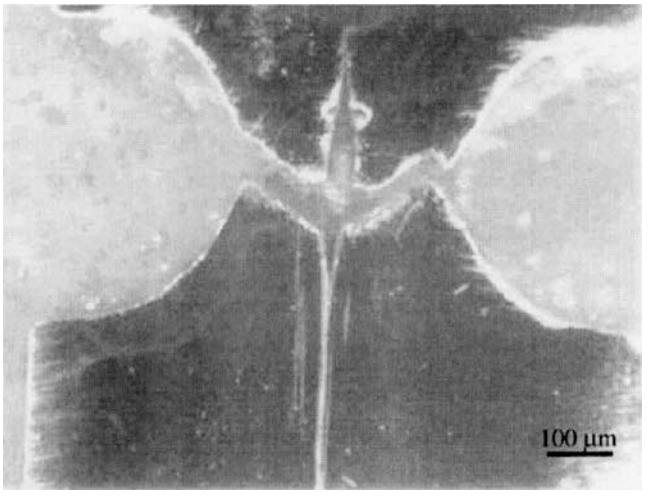

(*b*)

Fig. 1—Light microscopy images of (*a*) the fracture surface and (*b*) a transverse section of the fracture surface of a circumferentially notched specimen of AL-6XN specimen fractured at room temperature. Note large crack parallel to tensile axis.

III. RESULTS AND DISCUSSION

A. *Characteristics of the Microstructural Bands*

Our initial indication of the presence of microstructural banding in the AL-6XN came from a routine examination of the fracture surfaces of failed circumferentially notched specimens. While the typical cup-and-cone fracture surface characterized most of the specimens, the fracture surfaces of the high stress triaxiality ($R/\rho = 2$, "D-notch") specimens *split* along a plane parallel to the tensile axis, as seen in Figure 1. In these specimens, the failure process included one, and sometimes two, cracks growing along a plane(s) parallel to the tensile axis. Eventual specimen separation was thus characterized by a "splitting" crack intersecting the main fracture surface, as is readily apparent in Figure 1(b). Importantly, the less severely notched specimens, deforming at lower stress triaxiality ratios, did not show any evidence of fracture-surface splitting or crack growth parallel to the tensile axis. These specimens, which displayed considerably higher ductilities than the split D-notch specimens, failed after extensive necking with the typical cup and cone fracture surface. On the other hand, some degree of the splitting type of failure occurred in all of the high stress triaxiality, D-notched specimens, although the degree of splitting was more pronounced in those specimens oriented in the longitudinal direction of the plate.

In view of the tendency for only the severely notched specimens to split during failure, the material splitting behavior shown in Figure 1 appears to occur at an elevated level of stress triaxiality ratio (σ_m/σ_{eq}), where σ_m is the mean stress and σ_{eq} is the equivalent stress. For example, the splitting of the D-notched specimen, such as in Figure 1 occurred when $\sigma_m/\sigma_{eq} \approx 1.0$ for most of the deformation to failure. In contrast, the less severely notched specimens (that did not split) deform mostly at $\sigma_m/\sigma_{eq} \leq 0.8$. The higher level of stress triaxiality translates to a larger *transverse* stress component that is present in the most severely notched tensile specimens. Thus, specimen splitting occurs at significantly higher levels of transverse stresses, suggesting the presence of a "planar" microstructural feature oriented normal to the principal plane of fracture and sensitive to a transverse stress component. Consistent with this correlation is the recent observation of specimen splitting in initially smooth AL-6XN tensile specimens which form a pronounced neck during deformation.[22]

A closer examination of the cracks that propagate parallel to the tensile axis (Figure 2) reveals that the material splitting is the result of crack growth along a microstructural band that has a planar geometry and is roughly 100-μm thick in this case and located near the center of the specimen. Similar bands but not as thick are also evident in Figure 2(b). When viewed at higher magnifications, the bands consist of a high density of relatively *equiaxed* second-phase particles with sizes primarily in the 5 to 10 μm range and, occasionally, some "large" particles in the $\approx$50 μm range size. Many of the particles reside on grain boundaries stabilizing a smaller grain size ($\approx$10 μm) compared to that within the plate outside of the bands ($\approx$30 μm). The particles within the band are discrete and relatively uniformly spaced, unlike those observed in a 304L stainless steel by Tseng *et al.*,[12] where sigma phase forms in long stringers as elongated delta ferrite phase particles decompose upon heat treatment at 720 °C.

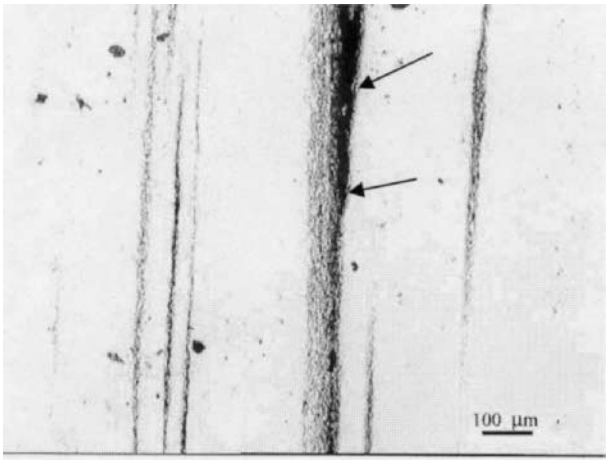

(*a*)

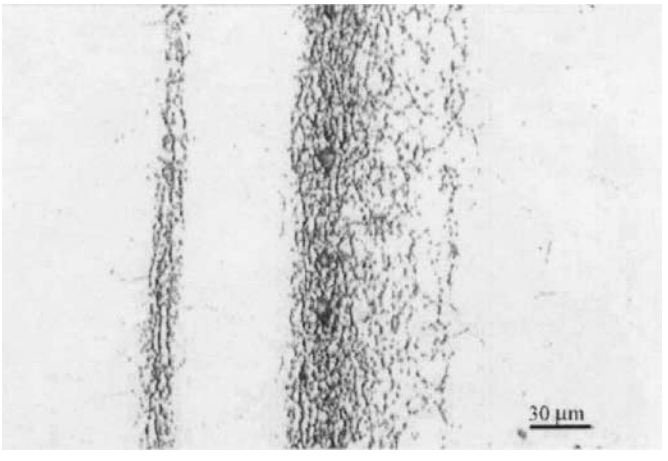

(*b*)

Fig. 2—Light micrographs depicting microstructural bands within the tensile specimen shown in Fig. 1. Note the arrested crack (arrows) that propagated along the large band in the center of (a).

The preceding observations, based on several "D-notched" tensile specimens, indicate that the AL-6XN plate contains microstructural bands located near the midthickness of the plate. An examination of eight different "edge" views of the as-received plate material confirms the presence of microstructural bands that range from a few microns to roughly 300 μm thick. The bands, which are located near the midthickness of the plate, are extended in length, especially in the rolling direction of the plate with many exceeding 10 mm in length and some as long as 50 mm.

The presence of a high density of second-phase particles within the microstructural bands and the tendency for crack growth along the bands suggest elevated hardness within the banded regions. Measurements from five different specimens, with a minimum of three indentations per band to obtain an average hardness, showed that the microstructural bands ranged in hardness from 300 to 360 VHN depending upon the density of the precipitates in the bands. In contrast, the hardness of the matrix was approximately 220 VHN. Thus, the microstructural bands have a significantly higher hardness than the matrix.

The material in Figure 2 was etched in a modified ASTM A262 etch (electrochemical oxalic acid procedure) designed to reveal sigma phase,[7] and thus, the etched image in Figure 2 suggests that the microstructural bands consist of a high density of sigma phase particles. Given the Mo- and Cr-rich chemistry of sigma phase in stainless steels, we expect that the bands should also show appropriate differences in chemistry from the neighboring particle-free matrix. In order to identify the differences in chemistry between the bands and the material adjacent to the bands, an EPMA was performed at several locations across the microstructural bands. The results, an example of which is shown in Figure 3, are based on data consisting of 100 measurements every 7 μm and indicate that the bands indeed contain high levels of Cr and Mo. When compared to the matrix composition, the banded region in Figure 3 shows an increase of Mo concentrations of up to 9 pct (by wt) at the maximum level near the center of the band; similarly, Cr contents increase within the band by increments of up to nearly 4 pct. Scans of other bands also indicate elevated levels of Mo and Cr contents, although the peak levels were usually lower than that shown in Figure 3. Also, some of the data, but not all, indicate elevated levels of Si. In contrast, Fe and Ni are depleted within the bands.

Also consistent with the sigma-phase hypothesis, electron dispersive spectroscopy analysis scans performed on several

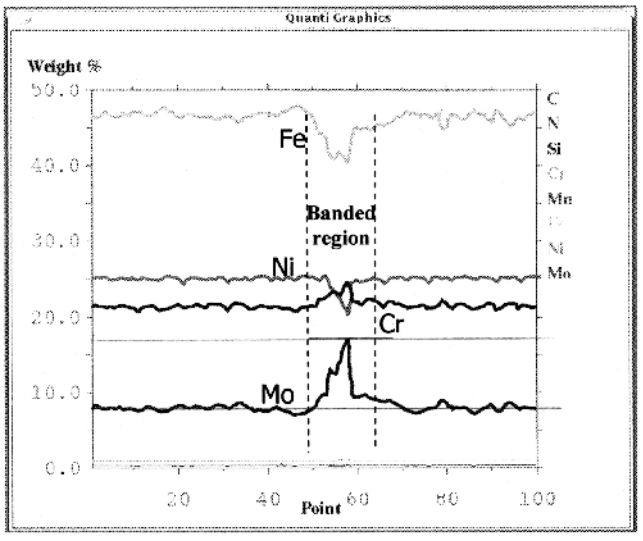

Fig. 3—Electron microprobe results over a 100-point (700-μm) scan that includes a large microstructural band with elevated levels of molybdenum and chromium and depleted levels of ferrite and nickel.

large, individual precipitate particles located on the fracture surfaces indicate elevated levels of Cr (typically 3 wt pct higher) and especially Mo (in excess of 10 wt pct higher) in the particles when compared to the matrix. Thus, these results suggest the likelihood of sigma phase being present in the microstructural bands. The elevated levels of Mo in particular suggest that these Mo-rich bands would be difficult to dissolve given the slow diffusion rate expected of Mo in this alloy.[23]

Stainless steels with high levels of Mo and Cr are known to be susceptible to the formation of intermetallic precipitates, most notably the sigma phase.[7–13] Sigma can be FeMo or FeCr, or it can have a variety of nonstoichiometric $(FeNi)_x(CrMo)_y$ compositions in stainless steels.[15] Sigma phase has a bcc tetragonal structure with, for example, lattice parameters of $a = 0.8790$ nm and $c = 0.4544$ nm for FeCr and $a = 0.9188$ nm and $c = 0.4812$ nm for FeMo.[24] In a study of a super austenitic stainless steel (Fe-22Cr-21Ni-6Mo-0.3N) conducted by Lee *et al.*,[25] they identified sigma phase with a tetragonal structure and lattice parameters of $a = 0.917$ nm and $c = 0.474$ nm, or somewhat similar to the FeMo sigma structure. In addition to Cr and Mo, silicon and titanium also aid in the formation of sigma,[14] while elements such as carbon, nickel, and nitrogen are used to retard its formation.[7,10,15,25] It should be recalled that in the results described previously, elevated levels of Cr and Mo, and in some cases Si, were found in the bands.

For stainless steels with high levels of Mo and Cr, previous research indicates that sigma may form when the material is cooled slowly through the 1040 °C to 650 °C temperature range[7,14] or during annealing at temperatures between 650 °C to 800 °C for a time period of a few hours.[10,15] Sigma phase can form directly from austenite or from decomposition of a ferrite phase that may form during solidification. According to Sutuala,[26] for stainless steels with a Cr_{eq}/Ni_{eq} ratio of less than 1.5, solidification is primarily austenitic. Since $Cr_{eq}/Ni_{eq} \approx 1.1$ for the base composition of AL-6XN, we would expect that if sigma phase formed, it would do so directly from the austenite. That sequence is consistent with the spatial distributions of particles and their near equiaxed shape in Figure 2. However, within the microstructural bands, the elevated levels of Mo and Cr, combined with a decrease of Ni, increase the Cr_{eq}/Ni_{eq} ratio in excess of 1.5, suggesting the possibility that delta ferrite forms on solidification and that sigma phase forms from the ferrite. (Nitrogen is a strong austenite stabilizer; but, unfortunately, the nitrogen levels within the bands are unknown.) Although we cannot rule out the possibility of ferrite formation, the equiaxed shape of the precipitates and the absence of precipitate stringers[12] suggest that the sigma phase forms directly from the austenite in our case.

Another intermetallic phase that may precipitate in AL-6XN is the chi phase.[24,25] The chi phase is a hard, brittle phase with a body-centered-cubic structure, whose lattice parameter is $a = 0.8920$ nm in the Fe, Cr, Ni, Mo system.[24] The two main compositions for the chi phase in austenitic stainless steels are $Fe_{36}Cr_{12}Mo_{10}$ and $(Fe,Ni)_{36}Cr_{18}Mo_4$. However, chi possesses an appreciable range of compositions with a high tolerance for metal interchange.[15,24] The morphology of this phase varies from rod-shaped to large globular particles, similar to that of the sigma phase. Also like sigma, chi forms first on grain boundaries, then on incoherent twins, and finally intragranularly.[15] The chi phase also tends to form during high-temperature aging, and its presence is greatly enhanced as the molybdenum content increases, consistent with the elevated levels of Mo observed in Figure 3. In view of the preceding discussion, in addition to the sigma phase, it is also possible that the chi phase is also present within the bands, given the variability in chemistries observed in the EPMA scans.

Orientation imaging microscopy (OIM) was used to identify the second-phase particles within bands that contained a high density of precipitates in the size range ≤ 10 μm. Based on OIM of the region shown in Figure 4, the second-phase particles are predominantly sigma phase ($\approx$0.23 area fraction), although there is also some chi phase present ($\approx$0.05 area fraction) in that scan. Our analyses of the OIM patterns assumed the following crystal structures: (a) sigma phase (tetragonal structure and lattice parameters of $a = 0.917$ nm and $c = 0.474$ nm)[25] and (b) chi phase (body-centered-cubic structure and a lattice parameter $a = 0.8920$ nm).[24] Other OIM scans of other banded regions confirmed that the second phase is predominantly the sigma phase. In some cases, chi phase was not present, and in other cases, some of the precipitate particles had crystal structures that could not be identified even though variations of the lattice parameters for the sigma and chi phases were assumed. Although a cursory examination did not detect delta ferrite,[12] it is possible that the unidentified particles were delta ferrite.

In summary, these observations indicate that the 12.7-mm-thick plate of AL-6XN examined in this study contains long (up to several millimeters) microstructural bands that have varying thicknesses ($\leq$300 μm) and are located near the midthickness of the plate and elongated in the rolling direction. The bands consist of a high density of second-phase particles (up to $\approx$30 vol pct) primarily based on the sigma phase. Given the presence of a significant volume fraction of hard intermetallic particles such as sigma or chi phase, it is no surprise that the bands are also significantly harder (VHN = 300 to 360 kg/mm^2) than the matrix (VHN = 225 kg/mm^2) and, as will be discussed in Section B, less ductile.

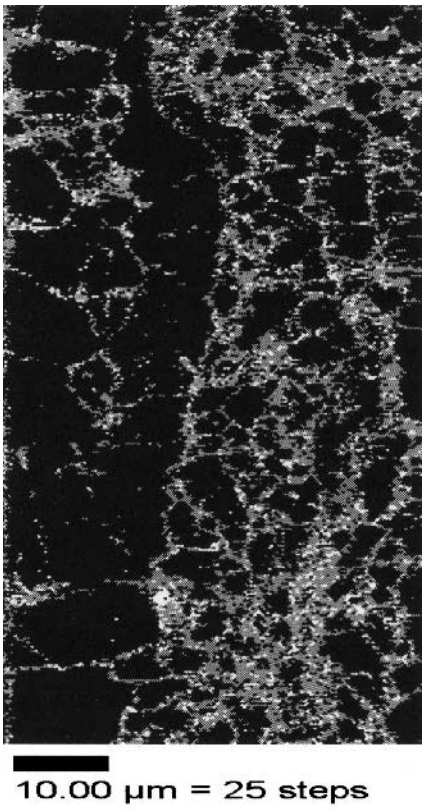

Fig. 4—OIM image showing microstructural banding in AL-6XN and indicating the following phases are present in the field of view above: ~72 pct austenite (black phase), ~23 pct sigma (gray phase), and ~5 pct chi phase (white phase).

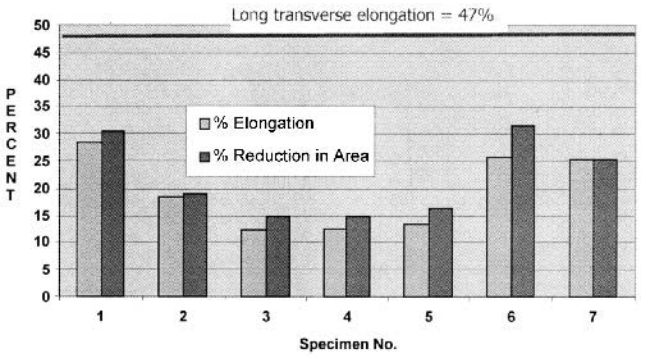

Fig. 5—Short transverse ductility data for seven AL-6XN specimens that contain microstructural bands. The tensile tests were performed with the tensile axis in the through-thickness orientation of the plate.

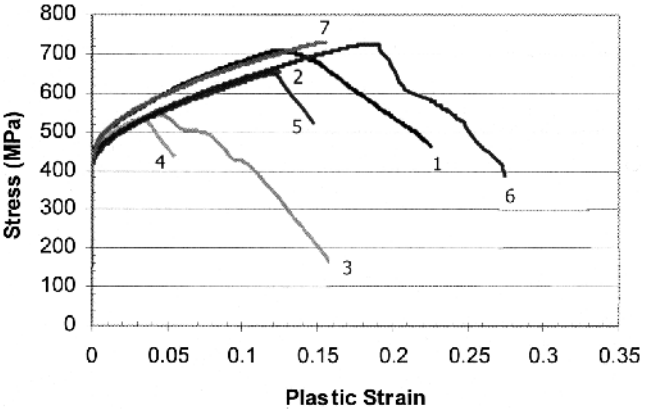

Fig. 6—The engineering stress-strain behavior of seven tensile AL-6XN specimens oriented in the short transverse direction.

B. *Effects of the Microstructural Bands on Tensile Ductility*

Our initial observation of the influence of microstructural banding on tensile fracture behavior was based on the previously described specimen splitting behavior that occurs *only* in the high triaxiality specimens ($\sigma_m/\sigma_{eq} \approx 1.0$ at failure). Those circumferentially notched specimens have specimen-to-specimen failure strains ($\varepsilon_f = 2 \ln (d_0/d_f) = 0.20$ to 0.31) that are much lower and also show much greater specimen-to-specimen variation than other specimens at lower stress triaxialities ($\sigma_m/\sigma_{eq} \leq 0.9$ at failure). All of these effects are direct results of the effects of the microstructural bands on the failure process.

In view of the planar geometry of the microstructural bands and similar to previous observations when sigma phase is present in plate material,[11,12] we would expect the tensile ductility of our AL-6XN plate to be especially low in the short-transverse orientation where the tensile direction is normal to the microstructural bands. As shown in Figure 5, the elongation to failure in the short-transverse orientation (a) is quite variable among the seven tests (ranging from 12 to 28 pct) and (b) is much lower than the 47 pct elongation to failure reported for tensile specimens tested in the long transverse orientation of the plate.[7] Furthermore, the load-displacement response shown in Figure 6 indicates that some of the specimens fracture abruptly while others fracture only after considerable extension after failure initiation (taken as the initial abrupt drop in load).

Examination of the fracture specimens shows that the specimens with lowest ductilities tend to have a flat fracture surface extending nearly across the entire specimen diameter, consistent with fracture primarily along a single band, such as shown in Figure 7(a). Importantly, the fracture surface of the low ductility specimens contains a high density of quite *large* (≈50 μm) particles (Figure 7(b)). These particles are present on a nearly continuous plane close to the midthickness of the plate and near the center of the gage sections of the tensile specimens. Thus, low ductility in the short transverse orientation is associated with the combination of an almost continuous band across the specimen width *and* the presence of large precipitate particles within that band.

In the case of short transverse specimens with high ductility, a rough fracture surface (Figure 8(a)) usually (but not always) forms during linking of fracture within discontinuous bands of *small* precipitates (≈10 μm), such as is shown in Figure 8(b). The rough topography of the surface suggests that cracks initiate within noncoplanar bands of precipitates and material fracture occurs only after extensive deformation along planes of high shear stress allows the cracks link to link.

The degree to which microstructural banding affects tensile failure in the through-thickness (short transverse) orientation can be readily understood using the schematic diagram shown in Figure 9. In this case, the specimen contains two discontinuous and noncoplanar bands of particles labeled

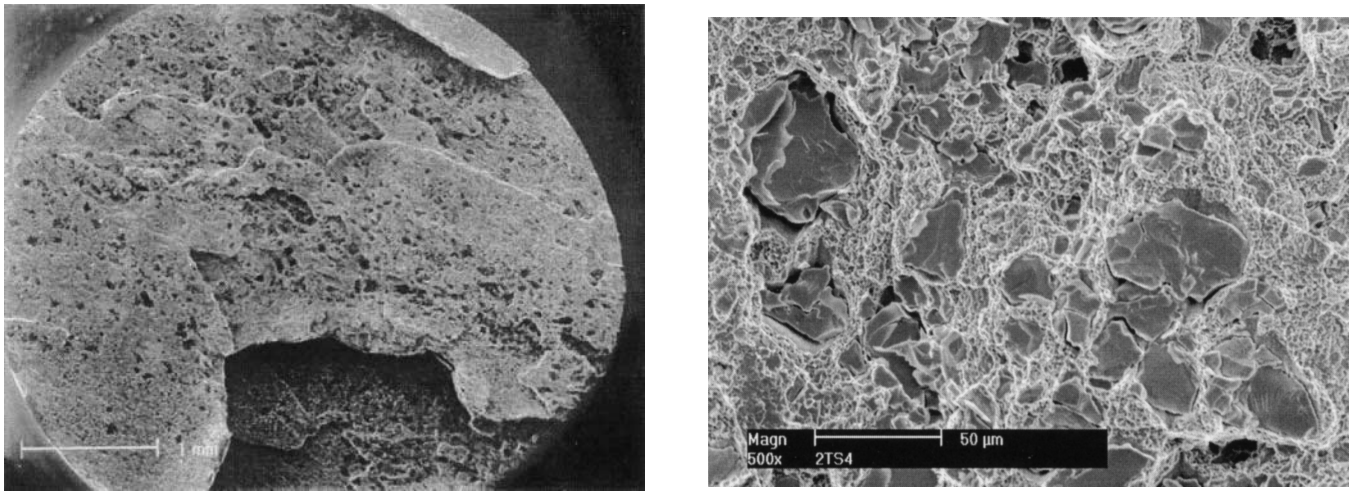

(*a*) (*b*)

Fig. 7—SEM fractographs of the low ductility specimen 4 showing (*a*) a relatively planar fracture surface and (*b*) a high density band of large (~50 μm) precipitates located near the fracture initiation region.

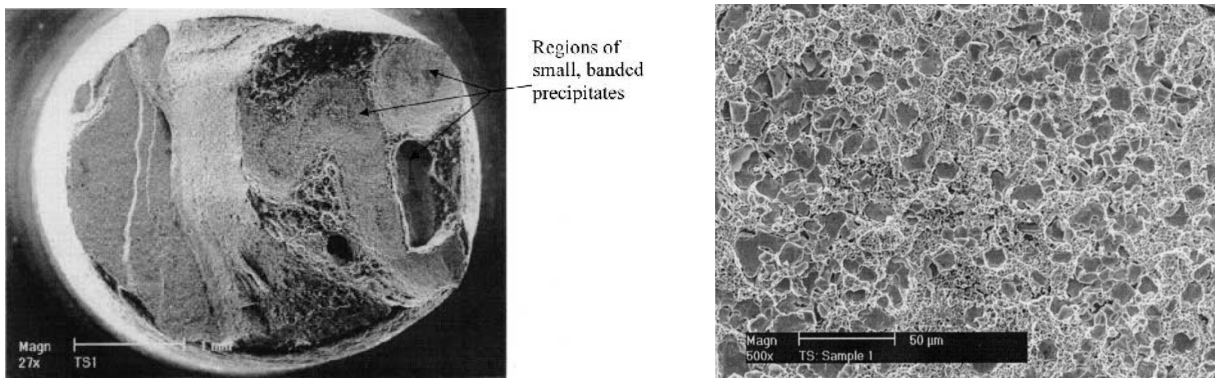

(*a*) (*b*)

Fig. 8—SEM fractographs of high ductility specimen 1 showing (*a*) a very rough, jagged fracture surface with pockets of small, banded precipitates; and (*b*) a high-magnification view of a band of small (~10 μm) particles.

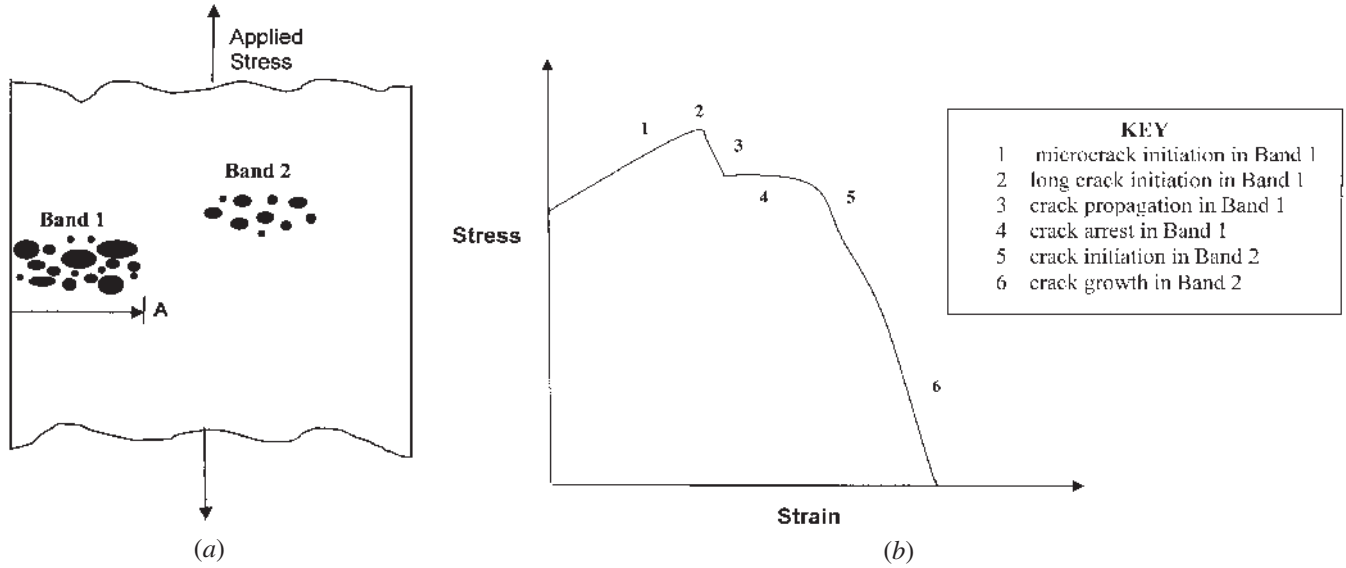

(*a*) (*b*)

Fig. 9—(*a*) A schematic illustration of a short-transverse tensile specimens containing two discontinuous and noncoplanar bands of particles, and (*b*) a schematic stress-strain curve illustrating the failure sequence occurring in (a).

band 1 (containing large particles) and band 2 (containing small particles) shown in Figure 9(a). Fracture is believed to occur in the following sequence.

1. A group of large precipitate particles located near the specimen surface in band 1 fracture forming a population of microcracks that link to form a long crack that arrests at the end of band 1 at location A.
2. The material continues to strain and eventually band 2 (with smaller particles) begins to crack.
3. Material fracture occurs after additional strain causes the linking of cracks within bands 1 and 2.

The preceding failure process is characterized by the load-displacement response shown schematically in Figure 8(b). Such a response is similar to that of the low-ductility specimen 3 in Figure 6 as well as the high ductility specimens 1 and 6. In these cases, fractography suggests that the ductility difference occurs because both of the low-ductility specimens (3 and 4) contain large particles ($\approx$50 μm) that initiate cracks at small strains. In contrast, the high-ductility specimens (specimens 1, 6, and 7) all have microstructural bands made up of small precipitate particles ($\approx$10 μm) that appear resistant to crack initiation.

An examination of the profile view of the fracture surface shown in Figure 10 confirms that large particles fracture in this case, at a crack initiation ($\varepsilon_c = 2 \ln d_0/d_f$) of $\leq$0.06. However, the small particles (0.5 to 2.5 μm) below the fracture surface (and near the edge of the microstructural band) do *not* crack or debond from the matrix. (Some etch pits formed around the small particles as a result of the etch attack used to delineate the particles.) Also, the absence of damage below the fracture supports our hypothesis of material fracture due to crack growth as opposed to a global damage accumulation process as is normally seen in the fracture of a ductile material during a tension test.

The failure process described previously implies that particle size is a critical factor in initiating fracture. Supporting this hypothesis are fractographic observations that show that the large particles frequently cracked, often at the base of a deep void, and usually with considerable void growth adjacent to them, suggesting considerable strain within the matrix after the particles fractured. On the other hand, an examination of smaller particles on the fracture surfaces of the more ductile specimens shows comparatively little void growth adjacent to them, suggesting that these particles are resistant to fracture and that material separation occurs shortly after particle fracture or debonding.

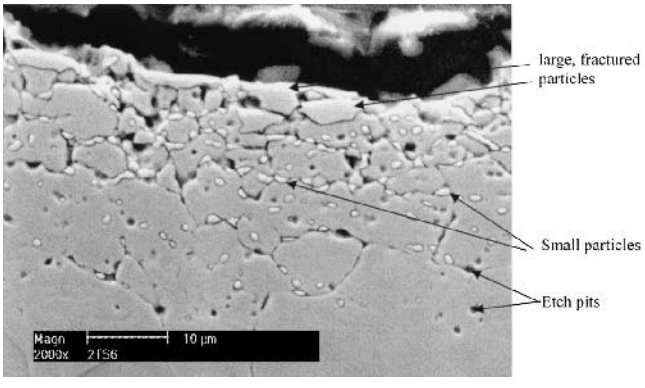

Fig. 10—SEM micrograph showing large, fractured precipitates along the fracture surface near fracture initiation, and a high density band of small precipitates below the surface. The precipitates below the surface appear to be unaffected by the specimen fracture.

For a wide range of metals and metal matrix composites, large particles are more likely to fracture at smaller strains, usually due to the increased probability of a pre-existing flaw being present in the larger particle. In the present study, we previously identified the small particles to be primarily sigma phase (Figure 4). Extensive quantitative energy dispersive analyses in the SEM on precipitate particles with varying sizes located on the fracture surface showed *no* differences in chemical composition, suggesting the large precipitates had the same structure as the small ones. Thus, these data suggest that precipitate size, and not a change in structure, likely dominates the increased susceptibility of the large particles to fracture at small strains.

In summary, the ductile fracture process that controls the ductility of the short transverse specimens involves crack initiation as second-phase particles (likely sigma phase) fracture within a microstructural band during deformation. The ease of crack initiation is promoted by increasing the size of the particles within a band, while the ease of crack propagation is promoted by increasing the length and continuity of the band.

IV. CONCLUSIONS

In our study of AL-6XN steel plate containing microstructural bands, we conclude the following.

1. Microstructural bands consisting of a high density of second-phase particles are present in the 12.7-mm-thick plate of AL-6XN. The bands have thicknesses ranging up to 300 μm and lengths often exceeding 10 mm; they are aligned in the rolling direction and located near the midthickness of the plate.
2. The microstructural bands have elevated levels of both chromium and molybdenum ($\leq$4 wt pct and $\leq$9 wt pct, respectively), and decreased levels of iron and nickel within the bands.
3. The second-phase particles within the bands are predominantly sigma phase $(Fe,Ni)_x(Cr,Mo)_y$ with $a = 9.17$ Å and $c = 4.74$ Å. Small levels of chi phase also appear to be present ($Fe_{36}Cr_{12}Mo_{10}$) in some bands.
4. The bands are harder than the matrix, having an average Vickers hardness between 300 and 360 kg/mm^2 (depending on the density of precipitates within the band) as compared to an average Vickers hardness of 225 kg/mm^2 in the matrix.
5. When oriented in either the long transverse or the longitudinal orientation of the plate, circumferentially notched specimens with mild notch geometries ($\sigma_m/\sigma_{eq} \leq 0.9$) are relatively insensitive to the presence of banding. However, fracture of more severely notched specimens ($\sigma_m/\sigma_{eq} \geq 1.0$) shows splitting parallel to the tensile axis, a much larger variation in the failure strains, and a significant reduction in tensile ductility.
6. The presence of the microstructural bands has a strong effect on the failure behavior of the tensile specimens oriented in the through-thickness, short transverse orientation of the plate. The tensile ductility of individual specimens is quite variable (from 7 to 24 pct) and much less than

the 47 pct reported for tensile specimens tested in the long transverse direction.

7. Failure of the short transverse tensile specimens occurs by a sequential process of crack initiation and crack growth. Crack initiation results from strain-induced fracture of large, brittle sigma particles, and crack growth occurs preferentially on a plane of high particle content. Thus, the presence of a *continuous* band of large precipitates severely limits ductility in the short-transverse orientation.

ACKNOWLEDGMENTS

The authors are grateful to John Grubb and David Begstrom for very helpful comments and insight, Maria Klimkiewicz for technical assistance in the OIM analyses, Ryan Wolfe for experimental assistance, and George Yoder for suggestions and enthusiastic support. This study was funded by the Office of Naval Research.

REFERENCES

1. J. Kirkaldy, J. Von Destinon-Forstmann, and R. Bingham: *Can. Metall. Q.*, 1962, vol. 1, pp. 59-81.
2. E.T. Turkdogan and R.A. Grange: *J. Iron Steel Inst.*, 1970, vol. 208, pp. 482-94.
3. S. Thompson and P. Howell: *Mater. Sci. Technol.*, 1992, vol. 8, pp. 777-84.
4. R.E. Reed-Hill and R. Abbashian: *Physical Metallurgy Principles*, PWS-Kent, Boston, MA, 1993, p. 459.
5. D. Chae, D.A. Koss, A.L. Wilson, and P.R. Howell: *Metall. Mater. Trans. A*, 2000, vol. 31A, pp. 995-1005.
6. T.F. Majka, D.K. Matlock, and G. Krauss: *Metall. Mater. Trans. A*, 2002, vol. 33A, pp. 1627-37.
7. Allegheny Ludlum: *AL-6XN Alloy*, 2nd ed., Allegheny Ludlum, Pittsburgh, PA, 1995.
8. P.A. Blenkinsop and J. Nutting: *J. Iron Steel Inst.*, 1967, vol. 67, pp. 953-58.
9. B. Weiss and R. Stickler: *Metall Trans.*, 1973, vol. 3, pp. 851-66.
10. J.R. Kearns and H.E. Deverell: *Mater. Performance*, 1987, vol. 26, pp. 18-28.
11. M.C. Mataya and M.J. Carr: *Deformation, Processing and Structure*, ASM, Materials Park, OH, 1982, pp. 448-59.
12. C.C. Tseng, Y. Shen, S.W. Thompson, M.C. Mataya, and G. Krauss: *Metall. Mater. Trans. A*, 1994, vol. 25A, pp. 1147-58.
13. M. Schwind, J. Kallqvist, J.O. Nilsson, J. Agren, and H.O. Andren: *Acta Mater.*, 2000, vol. 48, pp. 2473-81.
14. E.O. Hall and S.H. Agie: *Metall. Rev.*, 1966, vol. 11, pp. 61-88.
15. P. Marshall: *Austenitic Stainless Steel: Microstructure and Mechanical Properties*, Elsevier Applied Science Publishers Ltd., London, England, 1984, p. 30.
16. J.W. Hancock and A.C. Mackenzie: *J. Mech. Phys. Solids*, 1976, vol. 24, pp. 147-69.
17. G.R. Johnson and W.H. Cook: *Eng. Fract. Mech.*, 1985, vol. 21, pp. 31-48.
18. R. Batisse, M. Bethmont, G. Devesa, and G. Rousselier: *Nucl. Eng. Design*, 1987, vol. 105, pp. 113-20.
19. D.M. Goto, D.A. Koss, and V. Jablokov: *Metall Mater. Trans. A*, 1999, vol. 30A, pp. 2835-41.
20. B.L. Adams, S.I. Wright, and K. Kunze: *Metall. Trans. A*, 1993, vol. 24A, pp. 819-31.
21. "Introduction to Orientation Imaging Microscopy (OIM)," TSL Technical Note, TSL, Draper, UT, 2001.
22. J.B. McKirgan: Naval Surface Warfare Center, Carderock Division, West Bethesda, MD, unpublished research, 2003.
23. J. Grubb: Allegheny Ludlum Corp., Brackenridge, PA, unpublished research, 2003.
24. J. Steeds and J. Mansfield: *Convergent Electron Beam Diffraction of Alloy Phases*, Adam Hilger Ltd., Bristol, England, 1984, p. 27.
25. T. Lee, Y. Jung, and S. Kim: *Mater. Sci. Forums*, 1999, vols. 318–320, pp. 109-14.
26. N. Sutula: *Metall. Trans. A*, 1983, vol. 14A, pp. 191-97.